

Glassy dynamics in asymmetric binary mixtures of hard-spheres

Edilio Lázaro-Lázaro¹, Jorge Adrián Perera-Burgos², Patrick Laermann³, Tatjana Sentjabrskaja³, Gabriel Pérez-Ángel⁴, Marco Laurati^{3,5}, Stefan U. Egelhaaf³, Magdaleno Medina-Noyola^{1,5}, Thomas Voigtmann^{6,7}, Ramón Castañeda-Priego^{5,a} and Luis Fernando Elizondo-Aguilera^{7,b}

¹ Instituto de Física Manuel Sandoval Vallarta, Universidad Autónoma de San Luis Potosí, Alvaro Obregón 64, 78000, San Luis Potosí, San Luis Potosí, Mexico

² CONACYT - Unidad de Ciencias del Agua, Centro de Investigación Científica de Yucatán A.C. (CICY), Calle 8, No. 39, Mz. 29, S.M. 64, 77524, Cancún, Quintana Roo, Mexico

³ Condensed Matter Physics Laboratory, Heinrich Heine Universität, Universitätsstraße 1, 40225, Düsseldorf, Germany

⁴ Departamento de Física Aplicada, Cinvestav, Unidad Mérida, Apartado Postal 73 Cordemex, 97310, Mérida, Yucatán, Mexico

⁵ Departamento de Ingeniería Física, División de Ciencias e Ingenierías, Universidad de Guanajuato, Loma del Bosque 103, 37150, León, Mexico

⁶ Department of Physics, Heinrich Heine Universität Düsseldorf, Universitätsstraße 1, 40225, Düsseldorf, Germany and

⁷ Institut für Materialphysik im Weltraum, Deutsches Zentrum für Luft-und Raumfahrt (DLR), 51170, Köln, Germany*

(Dated: July 26, 2018)

The binary hard-sphere mixture is one of the simplest representations of a many-body system with competing time and length scales. This model is relevant to fundamentally understand both the structural and dynamical properties of materials, such as metallic melts, colloids, polymers and bio-based composites. It also allows us to study how different scales influence the physical behavior of a multicomponent glass-forming liquid; a question that still awaits a unified description. In this contribution, we report on distinct dynamical arrest transitions in highly asymmetric binary colloidal mixtures, namely, a single glass of big particles, in which the small species remains ergodic, and a double glass with the simultaneous arrest of both components. When the mixture approaches any glass transition, the relaxation of the collective dynamics of both species becomes coupled. In the single glass domain, spatial modulations occur due to the structure of the large spheres, a feature not observed in the two-glass domain. The relaxation of the *self* dynamics of small and large particles, in contrast, become decoupled at the boundaries of both transitions; the large species always displays dynamical arrest, whereas the small ones appear arrested only in the double glass. Thus, in order to obtain a complete picture of the distinct glassy states, one needs to take into account the dynamics of both species.

PACS numbers: 23.23.+x, 56.65.Dy

I. INTRODUCTION

The solidification of a liquid into an amorphous non-equilibrium glass is one of the most ubiquitous processes in nature, having also a remarkable scientific and technological relevance. Metallic alloys [1], bioactive materials [2], ceramics [3], polymers [4] and colloidal suspensions [5–9] are common examples of materials that under certain thermodynamic conditions are able to display a wide variety of non-crystalline structures and dynamically arrested states with solid-like properties that, so far, are not completely understood.

Acquiring full control of the physical properties of amorphous materials, however, requires to fundamentally understand how the solid-like behavior appearing in an undercooled glass-forming liquid is related to the dramatic slowing down of the microscopic dynamics [10, 11], and how such behavior is mediated by both the direct interactions among the particles and the thermodynamic conditions under which the material is prepared [12–14].

Model colloidal suspensions have played an important role in the study of glasses and gels, since they provide access to time and length scales at which most of the essential features of *glassy* behavior are manifested [15–18]. Colloids have noticeably improved our insight of the fundamental mechanisms for physical gelation [7–9] and the glass transition [5, 6], providing neat experimental realizations of dynamically arrested states in finely controlled systems and conditions [15, 16, 19–25]. One of the best known classes of colloidal model systems is the so-called *hard-spheres* (HS) dispersion. Despite their conceptual simplicity, colloidal HS are expected to retain many important features of glass-forming liquids near the dynamical arrest transitions [15, 16, 26, 27]. For a *monodisperse* HS suspension, the formation of glassy states at volume fractions $\phi \gtrsim 0.58$ is essentially due to a mechanism defined as “*caging*”, where the motions of individual particles are constrained by their nearest neighbors [15, 16, 28]. The addition of a second species with a different size, however, modifies drastically this scenario: for a narrow size disparity ($\delta \equiv \sigma_s/\sigma_b \gtrsim 0.4$; σ_s and σ_b being the diameters of the *small* and *big* particles, respectively), this implies a shift of the glass transition (GT) point to a larger total volume fraction [20], accompanied with spatial and temporal heterogeneities, and aging effects [12–14]. For higher degrees of asymmetry, and depending on the composition, different and more com-

*Electronic address: a)ramoncp@fisica.ugto.mx; Electronic address: b)luisfer.elizondo@gmail.com

plex glassy states, such as attractive and asymmetric glasses emerge [19, 24, 25, 29–33].

Attractive glasses and gels are observed in mixtures of HS colloids and non-adsorbing polymers [21–23] and, so far, they have been described almost invariably in terms of an effective one-component system; the presence of the polymers results in attractive depletion interactions among the colloidal particles [6–8, 34–37]. As we show in what follows, however, the glassy behavior of a highly asymmetric binary mixture of HS can only be fully understood by taking into account all the degrees of freedom of the two components, *i.e.*, one should consider explicitly the dynamical contribution of both species. This suggests that a description based, for example, on the depletion forces acting on the large species can only provide a coherent picture for the static correlations of an *effective* system composed of big attractive particles [38, 39], but cannot offer any insight on the fundamental relevance that the dynamics of the smaller species possesses in the GT of the mixture.

From a theoretical point of view, the GT in asymmetric HS mixtures has been described by the mode coupling theory (MCT) [40–43] and the self-consistent generalized Langevin equation (SCGLE) theory [44–47]. The predicted glassy scenario [48–51] agrees with experimental observations for the large spheres [24, 25]. Both approaches have predicted a richer and complex scenario for dynamical arrest, where the mobility of both species play a key role. Some of these features are in qualitative agreement with previous simulated results for binary mixtures of soft spheres [31–33]. However, to date no systematic and direct comparison between theory, simulation and experiments has been presented to corroborate the existence of different glassy states in highly asymmetric HS binary mixtures and to characterize in detail the *self* and collective dynamics of both species towards the distinct dynamical arrest transitions. This is the main goal of the present work.

Thus, in this contribution we unravel the dynamical mechanisms that lead to the different arrested states and provide a unified description of glassy dynamics in this model system. More specifically, we show how the glassy states differ in terms of the *self* and collective dynamics of both species, as well as the corresponding ergodicity parameters. We particularly emphasize the role of the small spheres, whose distinct relaxation patterns allow us to distinguish mixed glassy states (where only the large spheres undergo a GT), asymmetric glasses (where both species form a glass) and localization transitions of small particles in a glass of large spheres. We have performed extensive *event-driven* molecular dynamics (MD) simulations, developed theoretical calculations within the SCGLE formalism and performed confocal differential dynamic microscopy (DDM) experiments. A brief summary of the SCGLE theory, details of the simulations and experiments is provided in the supplemental material (SM).

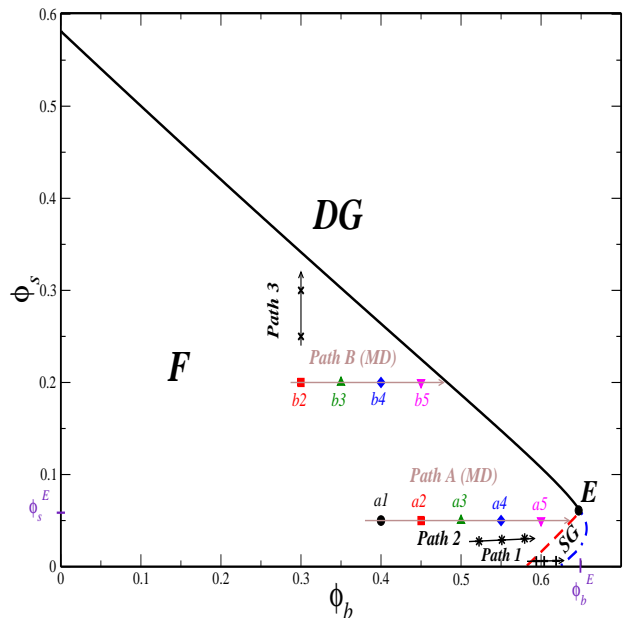


FIG. 1: (Color online) Dynamical arrest diagram for a binary mixture of HS with size ratio $\delta \approx 0.2$, as a function of the volume fractions of big, ϕ_b , and small, ϕ_s , spheres. Lines are predictions of the SCGLE theory [48] using the Percus-Yevick approximation [52] combined with the Verlet-Weiss correction [53] for the partial static structure factors. The (black) solid line indicates the transition from the fluid (F) to the *double* glass (DG). The (red) dashed line indicates the transition between the F and the *single* glass (SG). The (blue) dashed-dotted line shows the transition from the SG to the DG . The three transition lines intersect at the state point $E = (\phi_b^E, \phi_s^E)$. Two different paths obtained at constant ϕ_s are shown: *Paths A* ($\phi_s = 0.05$) and *B* ($\phi_s = 0.2$). The state points $a1$ – $a5$ and $b2$ – $b5$ along each path represents compositions studied with MD simulations. *Path 1* (+) corresponds to the experimental data of Ref. [29], whereas *Paths 2* (*) and *3* (x) correspond to experimental data obtained in this work.

II. ARRESTED STATES DIAGRAM OF A HIGHLY ASYMMETRIC BINARY MIXTURE OF HARD-SPHERES

We first present the dynamical arrest diagram of largely asymmetric binary mixtures of hard spheres with a size ratio $\delta \approx 0.2$ as a function of the control parameters (ϕ_b, ϕ_s) , *i.e.*, the volume fractions of, respectively, big and small spheres, as obtained by SCGLE (Fig. 1) [48]. Here $\phi_i \equiv \frac{\pi}{6} \rho_i \sigma_i^3$ ($i = s, b$), where $\rho_i \equiv N_i/V$ denotes the corresponding particle number density, and N_i the number of particles of species i in the volume V . For comparison, the diagram for $\delta \approx 0.1$ and experimental data previously reported in Ref. [25] are briefly presented and discussed in the SM.

Three different states can be distinguished: a fluid (F), where both species diffuse, a double glass (DG), in which both components are dynamically arrested, and a single glass (SG) where the big particles undergo a GT, whereas the small particles diffuse through the voids left by large spheres, similar to the case of tracer particles in crowded [29] and confining media [54]. It has been shown previously that the region of

mixed states, **SG**, expands when δ decreases, whilst it disappears for $\delta \gtrsim 0.38$ [48]. MCT provides qualitatively similar predictions [51].

The ergodic region **F** is enclosed by two different transitions: The transition from a fluid to a single glass (**F-SG**, red dashed) and the transition from a fluid to a double glass (**F-DG**, black solid). The **F-SG** line runs from $(\phi_b = 0.582, \phi_s = 0)$, *i.e.*, the GT point in the absence of small particles, to the *crossing point* labeled as $E \equiv (\phi_b^E, \phi_s^E)$. Along this line, ϕ_b monotonically increases with ϕ_s . This indicates that below ϕ_s^E , a glass can be *melted* upon the addition of small particles [20]. Above ϕ_s^E , in contrast, one encounters the **F-DG** line, extending from E to $(\phi_b = 0, \phi_s = 0.582)$. Along this line, ϕ_b monotonically decreases as a function of ϕ_s . In the limit of small ϕ_b , one observes a special type of *asymmetric* glass, where the large particles are localized in a glass of small spheres, as already observed in previous work [24]. Moreover, a third transition separates the single glass and double glass regions (**SG-DG**, blue dashed-dotted line). This transition describes the dynamical arrest of the small particles in the arrested large spheres.

For completeness, Fig. 1 also indicates the state points studied by means of MD simulations (*Paths A and B*) and DDM experiments (*Paths 1(+), 2(*) and 3(x)*), which are summarized in Table I.

<i>Path / Sample</i>	ϕ_b	ϕ_s	SCGLE	MD	EXP	Transition
A	0.40-0.60	0.05	✓	✓	×	F-SG
1.1	0.594	0.006	✓	×	✓	F-SG
1.2	0.6039	0.0061	✓	×	✓	F-SG
1.3	0.6138	0.0062	✓	×	✓	F-SG
2.1	0.5225	0.0275	✓	×	✓	F-SG
2.2	0.551	0.029	✓	×	✓	F-SG
2.3	0.5795	0.0305	✓	×	✓	F-SG
B	0.35-0.45	0.20	✓	✓	×	F-DG
3.1	0.3	0.25	✓	×	✓	F-DG
3.2	0.3	0.30	✓	×	✓	F-DG

TABLE I: List of the state points studied by means of SCGLE calculations, MD simulations and experiments for the transitions from the fluid (**F**) to the single glass (**SG**) and double glass (**DG**).

III. FLUID-GLASS TRANSITIONS (PREDICTED SCENARIO)

Let us first discuss the qualitative differences between the **F-SG** and **F-DG** transitions on the basis of characteristic quantities, such as the localization lengths and the non-ergodicity parameters, as predicted by the SCGLE formalism.

A. Localization length (self-dynamics)

In an ordinary HS glass, the mean square displacement (MSD) shows a long-time plateau [25], whose height indicates the displacement inside a *nearest-neighbors* cage. The

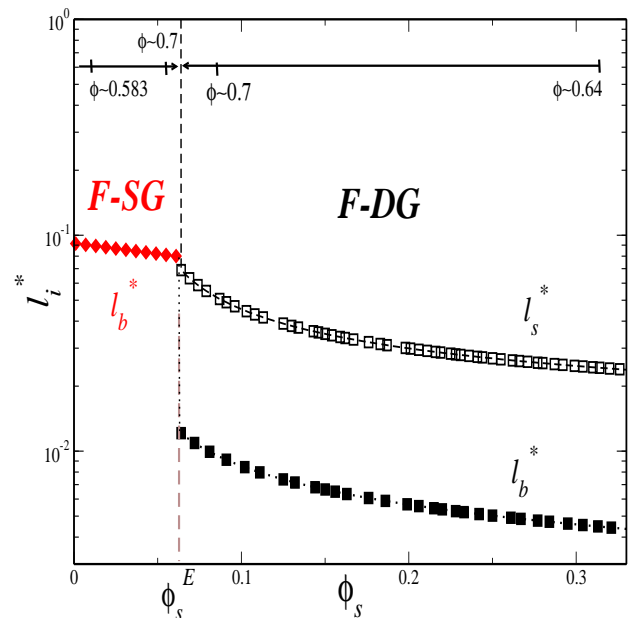


FIG. 2: (Color online) Normalized localization lengths l_b^* (solid symbols) and l_s^* (open symbols) of the large and small particles, respectively, as function of the volume fraction of small particles, ϕ_s , calculated with the SCGLE formalism along the two transition lines enclosing region **F** in Fig. 1.

square-root of this value is called localization length, l_i , and is a measure of the local confinement. In Fig. 2, the behavior of the localization lengths along the **F-SG** and **F-DG** lines is reported. For the **F-SG** transition ($0 \leq \phi_s \leq \phi_s^E$), the total volume fraction of the mixture, $\phi = \phi_b + \phi_s$, increases when going from the point $(\phi_b = 0.582, \phi_s = 0)$ to E , and the normalized localization length $l_b^* \equiv l_b/\sigma_b$ of the big spheres is found to be $l_b^* \approx 10^{-1}$. Hence, their characteristic *cage size* corresponds to approximately 10% of their diameter, a typical feature of an ideal glass of HS. On the other hand, the normalized localization length of the small particles, $l_s^* \equiv l_s/\sigma_b$, is infinite, indicating that the latter ones are not localized and diffuse (a feature not observed for a small degree of asymmetry [13]). These results suggest a dynamical decoupling of the *self* dynamics of both species.

At the intersection of the **F-SG** and **F-DG** lines, *i.e.*, at E , l_b^* discontinuously jumps from $\sim 10^{-1}$ to $\sim 10^{-2}$ and l_s^* becomes suddenly finite with a value $l_s^* \sim 10^{-1}$. This indicates that along the **F-DG** line, *i.e.*, for $\phi_s > \phi_s^E$, both species are localized, with the small particles being less localized than the large ones. The latter become even more localized than along the **F-SG** transition [24, 25] (see also SM). In this case, the total volume fraction ϕ decreases when going from E towards the point $(\phi_b = 0, \phi_s = 0.582)$. Both l_b^* and l_s^* become smaller with decreasing ϕ and increasing ϕ_s , which implies that the cage size along the **F-DG** line is controlled by the small spheres.

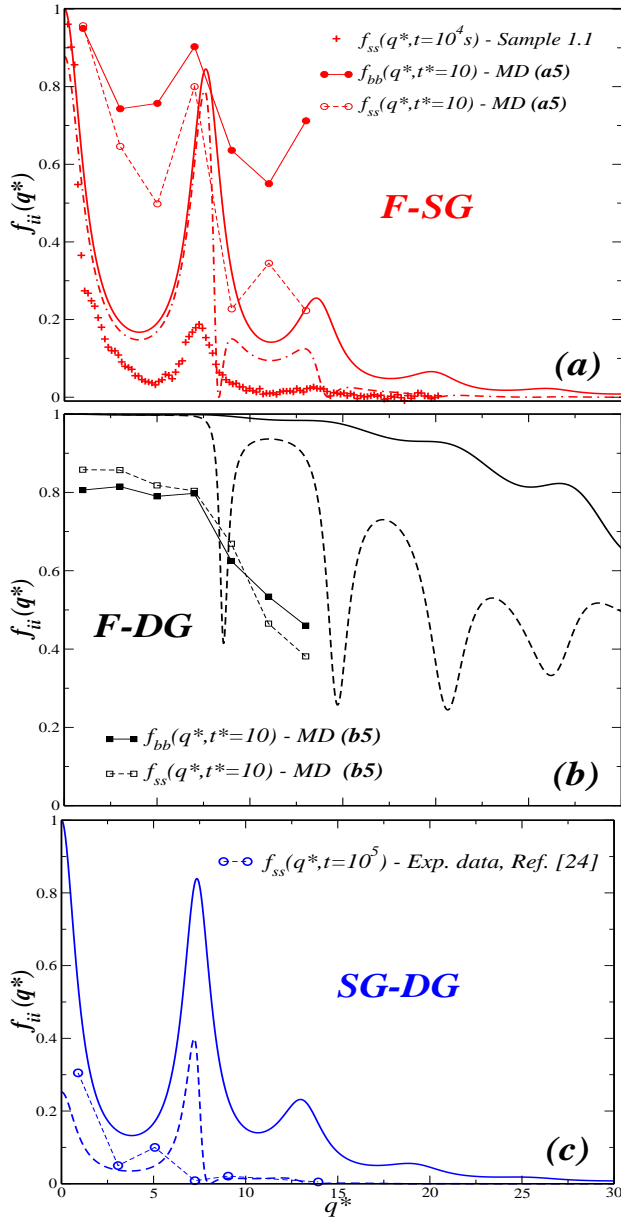


FIG. 3: (Color online) *Non-ergodicity* parameter (NEP) of the large particles, $f_{bb}(q^*)$ (solid lines), and of the small particles, $f_{ss}(q^*)$ (dashed-lines), as a function of the reduced wavenumber q^* as predicted by the SCGLE formalism: (a) at the intersection of *Path A* with the **F-SG** transition line; representative results extracted from the MD simulations at the state point *a5* and experimental data from Ref. [29] (Sample 1.1) are also displayed, (b) at the intersection of *Path B* with the **F-DG** transition line; representative results from the MD at the state point *b5* are shown, (c) at the intersection of *Path 1* with the **SG-DG** transition line.

B. Non ergodicity parameter (collective dynamics)

Another fundamental difference between the two transitions enclosing region **F** is characterized by the so-called *non ergodicity* parameters (NEP) [15, 16] $f_{ii}(q) \equiv \lim_{t \rightarrow \infty} F_{ii}(q, t)/S_{ii}(q)$, i.e., the *nondecaying* components of the

collective intermediate scattering functions (ISFs) $F_{ii}(q, t) = \langle \sum_{j,k}^N \exp(i\mathbf{q} \cdot [\mathbf{r}_j^{(i)}(t) - \mathbf{r}_k^{(i)}(0)]) \rangle / N$, where \mathbf{q} is the scattering vector, $\mathbf{r}_j^{(i)}(t)$ describes the position of the j -th particle of species i at time t , and $S_{ii}(q)$ denotes the corresponding partial static structure factor ($S_{ii}(q) = F_{ii}(q, t = 0)$). The emergence of non-zero values for $f_{ii}(q)$ is associated with the dynamical arrest of the collective dynamics of species i .

Fig. 3 shows the predictions of the SCGLE theory for the NEP of the big, $f_{bb}(q^*)$, and small, $f_{ss}(q^*)$, particles at three points located on the (a) **F-SG**, (b) **F-DG** and (c) **SG-DG** lines as a function of the reduced wave number $q^* \equiv q\sigma_b$. In order to later compare with the simulation results, we have chosen the points on the **F-SG** and **F-DG** lines that correspond to the crossing points with the two paths investigated with MD, indicated as *Paths A* and *B*. Similarly, we have considered the *Sample 1.1* (see Table I), which almost intersects the transition line **F-SG**.

For the point at the intersection of *Path A* with the **F-SG** transition line (Fig. 3 (a)), one observes an oscillatory behavior in both $f_{bb}(q^*)$ and $f_{ss}(q^*)$, associated with modulations of the structure factor of the big species, $S_{bb}(q^*)$. Both NEPs appear coupled and they are essentially identical up to $q^* \approx 7.18$, which approximately corresponds to the location of the main peak of $S_{bb}(q^*)$. Thus, at large length scales, the collective dynamics of the small spheres is controlled by the confinement of the large particles. For $q^* > 7.18$, oscillations are still present, but become decoupled. The NEPs cease to oscillate and decay to nearly zero at values $q^* \approx 20$ in the case of $f_{ss}(q^*)$ and $q^* \approx 30$ for $f_{bb}(q^*)$. This indicates that, at smaller length scales, the small spheres can explore the local environment. Data for both NEPs obtained from MD simulations at long time ($t^* = 10$), and for $f_{ss}(q^*)$ obtained from DDM experiments (at $t = 10^4s$) shows also oscillations at comparable q^* values. This will be discussed in detail below (see, for instance, Figs. 7 and 10).

In contrast, for the point at the intersection of *Path B* with the **F-DG** transition line (Fig. 3(b)), one observes a different behavior. Both $f_{bb}(q^*)$ and $f_{ss}(q^*)$ appear coupled for $q^* \leq 7.18$, but now remain constant at about unity. For $q^* > 7.18$, the NEPs are decoupled and large oscillations appear only in $f_{ss}(q^*)$. Also, larger *spectra* of non-decaying components in the ISFs of both species are observed up to $q^* \approx 150$ (not shown). NEPs obtained from MD simulations are also constant for $q^* < 7.18$, but decay for larger q^* and appear coupled. This will also be discussed below (see Fig. 14).

In Fig. 3(c), the SCGLE predictions for the behavior of the NEPs at the intersection of the **SG-DG** transition line with *Path 1* are shown. The behavior is qualitatively similar to that observed at the **F-SG** transition, but $f_{ss}(q^*)$ is noticeable smaller than $f_{bb}(q^*)$ for $q^* \leq 7.18$, and becomes nearly zero for $q^* > 7.18$ (note that along *Path A* $\phi_s = 0.05$, whereas along *Path 1* $\phi_s \approx 0.0062$). Hence, at this transition the small particles become trapped in voids created by big particles, thus resembling a localization transition in random porous media [54].

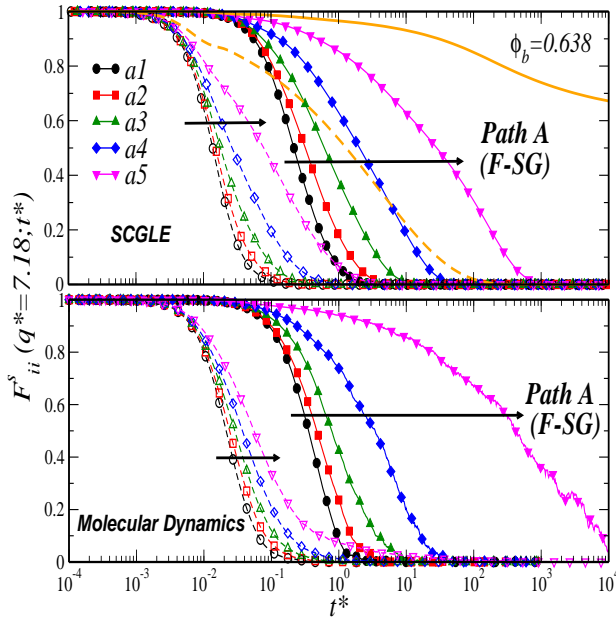


FIG. 4: (Color online) Self ISFs for the large, $F_{bb}^S(q^*, t^*)$ (solid symbols), and small particles, $F_{ss}^S(q^*, t^*)$ (open symbols), calculated along *Path A* (as indicated) at fixed $q^* = 7.18$ and as a function of the reduced time $t^* \equiv t/t_b^0$, where $t_b^0 = \sigma_b \sqrt{M_b}/k_B T$, M_b is the mass of any of the large particles, k_B the Boltzmann constant and T the absolute temperature (Ref. [55] and SM). The upper panel displays the results of the SCGLE theory (including the (orange) solid and dashed curves for, respectively, the big and small particles, at the critical value $\phi_b^{(g)} = 0.638$) and the lower panel shows results of MD simulations.

IV. DYNAMICS FROM THE FLUID TO THE SINGLE GLASS

We have investigated the dynamics of the mixture towards the *F-SG* transition by means of theory, simulations and experiments. We have carried out *event-driven* MD simulations with $\delta = 0.2$ and following *Path A*, *i.e.*, fixing $\phi_s = 0.05$ and varying ϕ_b . In the experiments, we have studied mixtures with $\delta \approx 0.18$ and followed two different trajectories at fixed composition of the small species, namely, $x_s \equiv \phi_s/\phi = 0.01$ (*Path 1*) and $x_s = 0.05$ (*Path 2*), and varied the total volume fraction ϕ . Details of the simulations and experiments are provided in the SM and Ref. [55].

A. Self dynamics at the *F-SG* transition

Fig. 4 displays a comparison between the SCGLE predictions (upper panel) and MD results (lower panel) for the behavior of the *self* ISFs, $F_{ii}^S(q, t) \equiv \langle \exp[i\mathbf{q} \cdot \Delta\mathbf{R}^{(i)}(t)] \rangle$, along *Path A* and evaluated at $q^* = 7.18$; where $\Delta\mathbf{R}^{(i)}(t)$ denote the displacement of *any* of the N_i particles of species $i (= b, s)$ over a time t . To allow for a one-to-one comparison between the SCGLE results and the MD simulations, we have appealed to the *molecular* version of the SCGLE theory [55].

The *self* ISFs obtained from SCGLE decay much faster

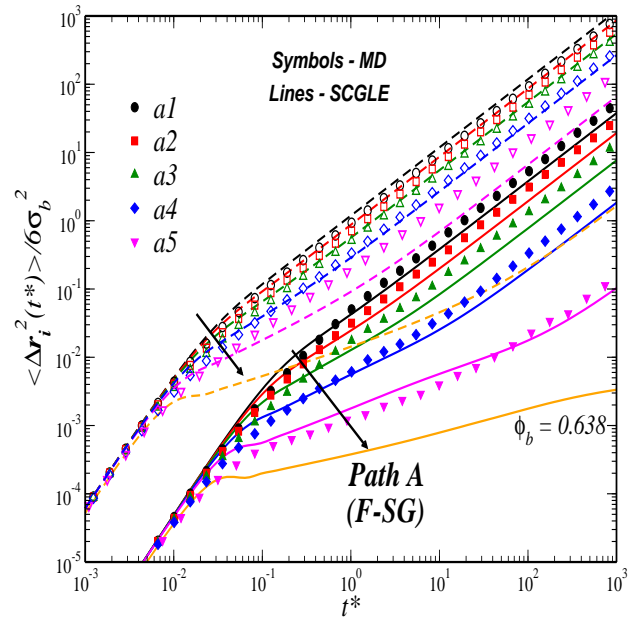


FIG. 5: (Color online) MSDs for the large (solid symbols and solid lines) and small particles (open symbols and dashed lines) along *Path A* (as indicated) obtained from MD simulations (symbols) and the SCGLE theory (lines).

for the small than for the large spheres. Upon increasing ϕ_b , a general slowing down is observed with the difference between the relaxation times of small and big particles strongly increasing. Nevertheless, the *self* ISF of the small species always decays to zero, as expected (Sec. III A). In contrast, the relaxation of $F_{bb}^S(q^* = 7.18; t)$ becomes much slower and, at the critical volume fraction $\phi_b^{(g)} = 0.638$ (orange solid line), it develops the characteristic two-steps relaxation in the dynamics (this state point has no counterpart in the simulations). Thus, the only signature of dynamical arrest appears for the large species.

The above scenario qualitatively agrees with the MD simulations (lower panel of Fig. 4), although with some differences. For instance, at the state point *a5*, both theory and simulations show a pronounced decoupling. However, the MD results reveal a slower relaxation of the large spheres and a slightly different final relaxation of the small ones. The latter reminds on the dynamical landscape of tracers in crowded environments, for instance, diffusion in heterogeneous porous media [54]. At this stage, we should point out that the MD simulations at *a5* disclosed the structure of the large particles similar to that of a highly amorphous material, see, e.g., SM, which nevertheless exhibits a particle dynamics reminiscent of a GT.

Fig. 5 presents the corresponding MSDs obtained from MD and SCGLE. The features of the *self* ISFs are also manifested in the corresponding MSDs $W_i^*(t; \phi_b, \phi_s) \equiv \langle (\Delta\mathbf{r}_i(t))^2 \rangle / 6\sigma_b^2$, ($i = s, b$). For instance, at intermediate and long times, the MSD of the smaller particles decreases approximately one order of magnitude when increasing ϕ_b along *Path A*, whereas the MSD of the large particles decreases by more than two or-

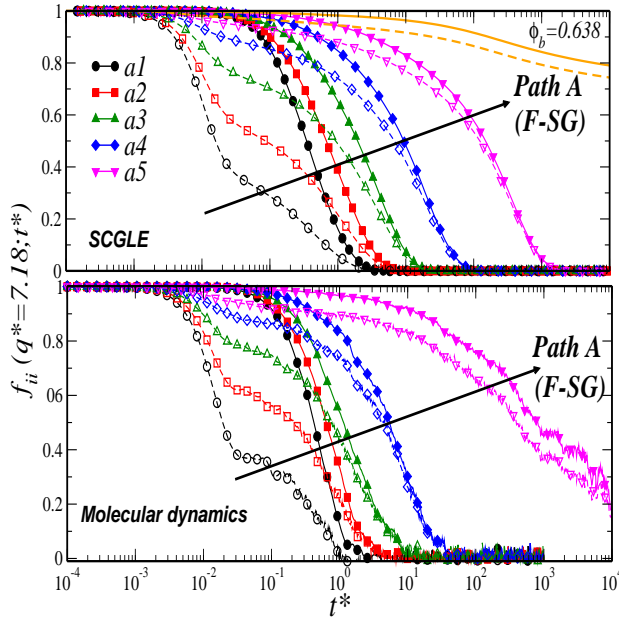


FIG. 6: (Color online) Normalized collective ISFs for the large, $f_{bb}(q^*, t^*)$ (solid symbols), and small particles, $f_{ss}(q^*, t^*)$ (open symbols), calculated along *Path A* (as indicated) at fixed $q^* = 7.18$ as a function of the reduced time t^* . The upper panel displays the results from the SCGLE theory and the lower panel from MD simulations.

ders of magnitude and exhibits an increasingly extended subdiffusive regime at intermediate times. This is in agreement with the physical scenario outlined in Fig. 2.

B. Collective dynamics at the *F-SG* transition

We now turn to the *normalized* collective ISFs, $f_{ii}(q, t) \equiv F_{ii}(q, t)/S_{ii}(q)$. Fig. 6 displays the predictions of the SCGLE (upper panel) and MD data (lower panel) for $f_{ii}(q^* = 7.18, t^*)$ along *Path A*, which both provide essentially the same scenario. The behavior of f_{bb} is very similar to F_{bb}^S (see Fig. 4). Instead, f_{ss} noticeably differs from F_{ss}^S . At the state point *a1*, for instance, the former exhibits a two-step relaxation not observed in the latter. Upon increasing ϕ_b , however, f_{ss} gradually evolves and eventually follows the same trend as f_{bb} . Thus, approaching the *F-SG* transition the *normalized* collective ISFs of both species become slower and coupled at wavenumbers $q^* = 7.18$, as discussed above (Fig. 3(a)). These features are qualitatively the same in both SCGLE and MD results, although the latter show a slower relaxation with respect to the former at the state point *a5*.

A few remarks might be in order. As mentioned before, the *SG* domain describes a region of partially arrested states, where the large spheres are predicted to undergo dynamical arrest and the small ones remain ergodic. At the level of *self* diffusion quantities, this feature of the *F-SG* transition was observed through the decoupling of the self ISFs, F_{bb}^S and F_{ss}^S , and of the MSDs, $W_b(t)$ and $W_s(t)$ (Figs. 4 and 5, respectively). At the level of collective dynamics, however, there

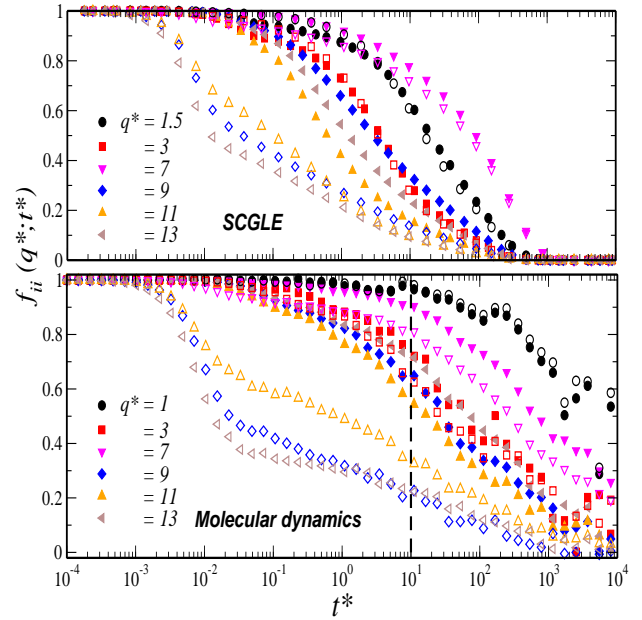


FIG. 7: (Color online) Normalized collective ISFs for the large, $f_{bb}(q^*, t^*)$ (solid symbols), and small particles, $f_{ss}(q^*, t^*)$ (open symbols), at the state point *a5* ($\phi_b = 0.60, \phi_s = 0.05$), for different q^* (as indicated) as a function of the reduced time, t^* obtained from the SCGLE theory (upper panel) and MD (lower panel). The vertical dashed line in the lower panel indicates $t^* = 10$, at which the values $f_{ii}(q^*, t^* = 10)$ have been extracted for the comparison in Fig. 3.

is a subtle feature that deserves to be briefly commented. To describe collective diffusion, one conventionally considers the *normalized* ISFs, f_{bb} and f_{ss} , which are quantities accessible experimentally. According to Fig. 6, both ISFs display a slowing down in the relaxation and become strongly correlated towards the *F-SG* transition, thus suggesting the deceiving notion that, at the level of collective variables, it is only possible to detect either fluid or arrested states but not partially arrested ones. Nonetheless, this is only the result of the convention adopted to describe collective diffusion. To see this, one may consider the *propagator* matrix $\Psi(q, t) \equiv F(q, t)S^{-1}(q)$, with initial condition $\Psi(q, t = 0) = I$. In terms of the diagonal *propagators* $\Psi_{bb}(q, t)$ and $\Psi_{ss}(q, t)$, the scenario for the collective dynamics of the *F-SG* transition differs from that displayed by $f_{bb}(q, t)$ and $f_{ss}(q, t)$. Specifically, one finds that the collective propagator $\Psi_{bb}(q^* = 7.18, t)$ displays dynamical arrest, whereas $\Psi_{ss}(q^* = 7.18, t)$ decays to zero, in qualitative similitude with the behavior of the *self* ISFs (for a detailed discussion, the reader is referred to Sec. IV of Ref.[48] and the SM).

We have additionally analyzed the q^* -dependence of $f_{ii}(q^*, t^*)$ for the sample closest to the *F-SG* transition along *Path A*, *i.e.*, the state point *a5*. As shown in Fig. 7, both f_{bb} and f_{ss} display an initial acceleration of the decay with increasing q^* , a slowing down for $q^* = 7$, and a second acceleration for larger q^* . These effects are attributable to the modulation of the structure factor of the large particles, as already mentioned (Fig. 3(a)). Additionally, for $q^* > 7$, f_{ss}

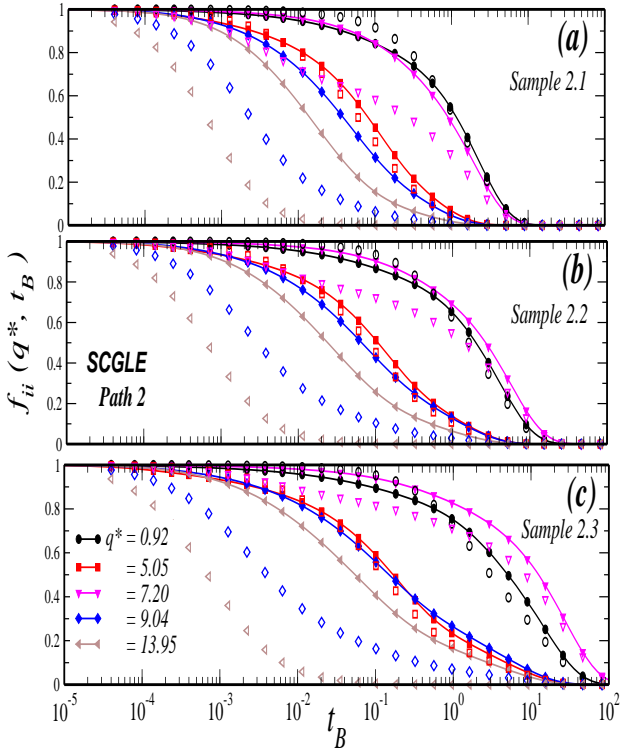


FIG. 8: (Color online) Normalized collective ISFs for the large, $f_{bb}(q^*, t_B)$ (solid symbols), and small particles, $f_{ss}(q^*, t_B)$ (open symbols), along *Path 2* (Samples (a)2.1, (b)2.2, (c)2.3) for different wave numbers q^* (as indicated) as a function of time $t_B \equiv t/D_b^0\sigma_b^{-2}$ predicted by the SCGLE theory.

develops distinct relaxation patterns as those observed in f_{bb} ; a faster initial decay followed by an intermediate inflection point, whose height *oscillates* with increasing q^* . This reflects the increasingly smaller fraction of small particles that are temporarily trapped at increasingly shorter length scales (larger q^* values).

To test the influence of ϕ_s on the q^* -dependence of the dynamics, theoretical and experimental data along *Path 2* ($\phi_s \approx 0.03$) are reported in Figs. 8 and 9, respectively. The SCGLE predicts a similar scenario as that found for $\phi_s = 0.05$, involving a non-monotonic behavior in the relaxation of both species upon varying q^* . Despite the smaller time resolution of the experiments, the measured ISFs show similar trends. The SCGLE and experimental results suggest different decay patterns and transient plateaus of f_{ss} for $q^* \approx 9$, although with some quantitative differences that become larger with increasing ϕ_b , *i.e.*, approaching the transition line, thus suggesting a void structure slightly different in the theoretical and experimental samples.

To further investigate the influence of both ϕ_s and ϕ_b on the height of the intermediate plateaus of $f_{ss}(q^*, t)$, we also consider *Path 1*, which corresponds to experimental data previously reported for $\phi_s \approx 0.006$ [29] and, according to the theory, located inside the *SG* domain. The results displayed in Fig. 10 show that, in comparison to the previous case ($\phi_s \approx 0.03$), the height of the plateaus in f_{ss} are generally

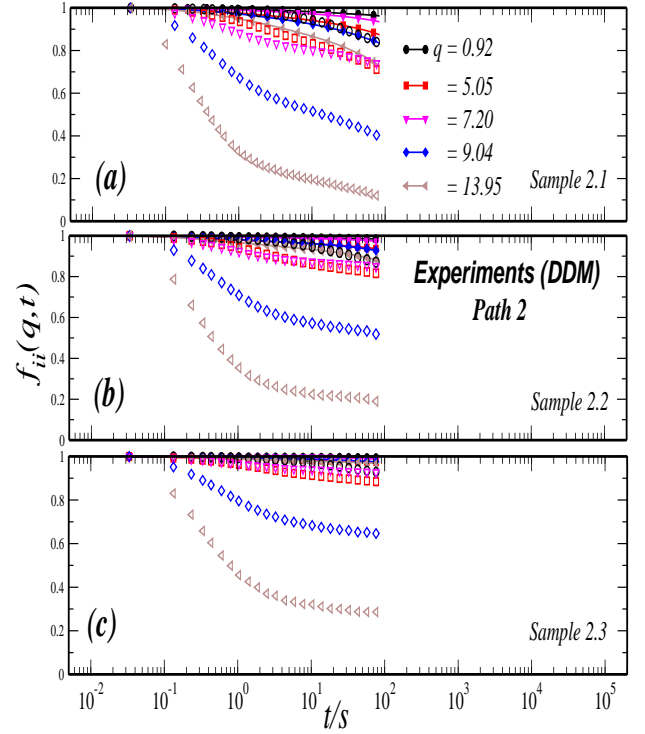


FIG. 9: (Color online) Normalized collective ISFs for the large, $f_{bb}(q^*, t)$ (solid symbols), and small particles, $f_{ss}(q^*, t)$ (open symbols), along *Path 2* (Samples (a)2.1, (b)2.2, (c)2.3) for different wave numbers q^* (as indicated) as a function of time t as observed in experiments.

shorter at comparable q^* values; a feature that was already outlined by the SCGLE theory in Fig. 3(c). This implies that due to crowding, *i.e.*, increasing ϕ_s , localization involves a larger fraction of small particles down to smaller length scales.

In summary, approaching the *F-SG* transition ($\phi_s < \phi_s^E$), the *self* dynamics of the small and large particles decouples, with the large particles approaching dynamical arrest. On the other hand, the collective ISFs of both species are coupled at long times, with the small spheres following the arrest of the larger ones. In addition, their wave number dependence is modulated by the structure of the large particles.

V. DYNAMICS FROM THE FLUID TO THE DOUBLE GLASS

We now discuss the dynamical features of the *F-DG* transition. Theory and simulation results for constant $\phi_s = 0.2$ and increasing ϕ_b from the fluid region towards the *F-DG* transition line (*Path B*) are discussed. These results are complemented with results from DDM experiments (*Path 3*).

A. Self dynamics of the *F-DG* transition

Fig. 11 reports *self* ISFs for fixed $q^* = 7.18$ and along *Path B* as obtained by theory and simulations. Different from

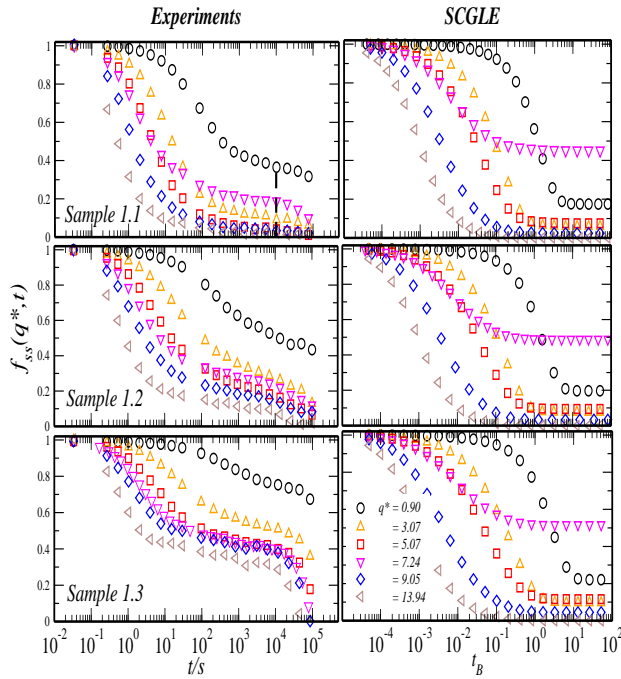


FIG. 10: (Color online) Normalized collective ISFs of the small species, $f_{ss}(q^*, t)$, along *Path 1* for different values of q^* . Left column: experimental results reported in Ref. [29]. Right column: SCGLE predictions. The vertical dashed line in (a) indicates the time, $t = 10^4$ s, at which the values $f_{ss}(q^*, t = 10^5$ s) were extracted for the comparison shown in Fig. 3(a).

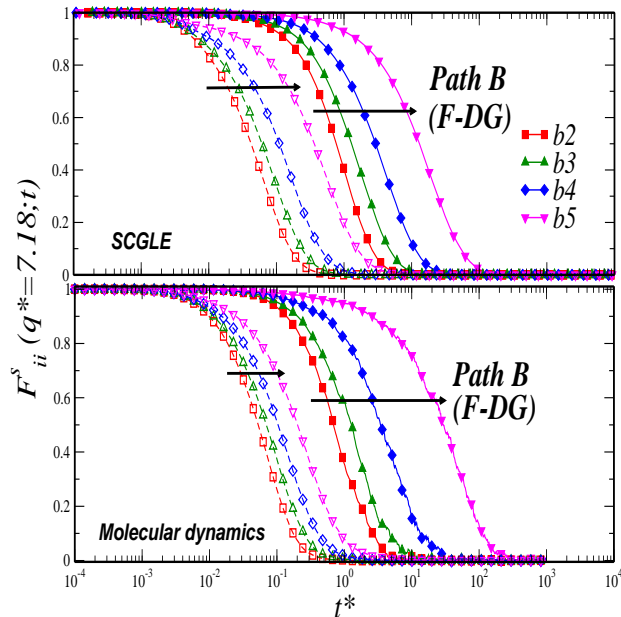


FIG. 11: (Color online) Self ISFs for the large, $F_{bb}^S(q^*, t^*)$ (solid symbols), and small particles, $F_{ss}^S(q^*, t^*)$ (open symbols), calculated along *Path B* (as indicated) at fixed $q^* = 7.18$ and as a function of the reduced time t^* . The upper panel displays the results of the SCGLE theory and the lower panel shows results of MD simulations.

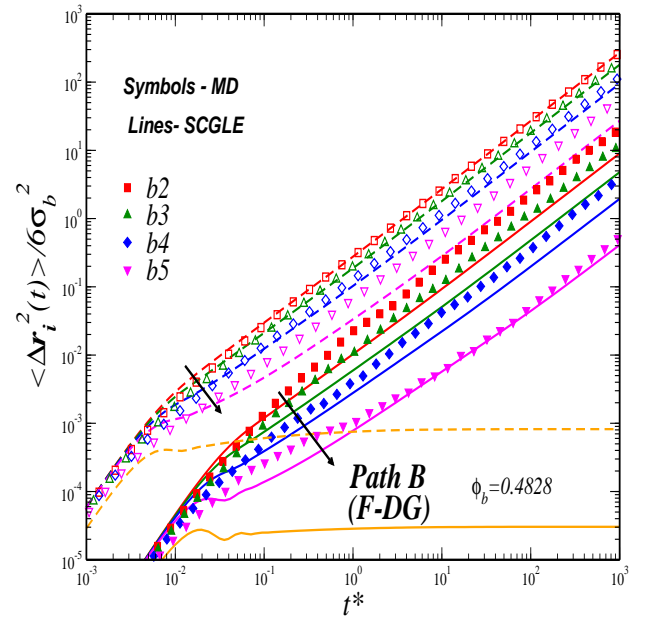


FIG. 12: (Color online) MSDs for the large (solid symbols and solid lines) and small particles (open symbols and dashed lines) along *Path B* (as indicated) obtained from MD simulations (symbols) and the SCGLE theory (lines).

the case of approaching to the *F-SG* transition (Fig. 4), the shape of the *self* ISFs of both species is rather similar, but with a faster decay for the small particles. Upon increasing ϕ_b , both ISFs slow down by a similar factor. No signature of a two-step decay in F_{bb}^S or a long-time tail in F_{ss}^S is observed. These results reflect the *lubricating* effect of the large enough fraction of small particles on the big particles (compare, for instance, the behavior of F_{bb}^S at the two state points *a5* (Fig. 4) and *b5*, both of which satisfy $\phi_s + \phi_b = 0.65$), as suggested by previous experimental studies [12–14, 16, 20, 24, 25].

These results are in agreement with the corresponding MSDs shown in Fig. 12. Again, along *Path B* the slow down of the small and large particles is very similar, in contrast to the very different slow down found along *Path A*.

B. Collective dynamics of the *F-DG* transition

The collective dynamics obtained by simulations and theory are displayed in Fig. 13. For the large particles, $f_{bb}(q^* = 7.18; t^*)$ behaves quite similar to the *self* part, $F_{bb}^S(q^* = 7.18; t^*)$, and also decays faster in comparison to the behavior along *Path A*. In contrast, for the small particles, $f_{ss}(q^* = 7.18; t^*)$ is different to $F_{ss}^S(q^* = 7.18; t^*)$, but also to the behavior found along *Path A*. The collective ISF of the small species now show a relaxation pattern that, from intermediate times onwards, resembles that of the large particles f_{bb} . Approaching the *F-DG* transition, these correlation functions become increasingly similar and eventually are essentially indistinguishable.

We also consider the q^* -dependence of the most concen-

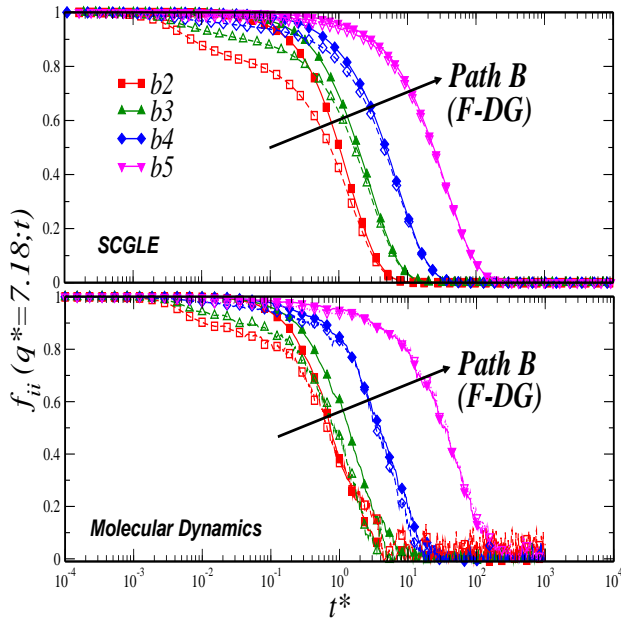


FIG. 13: (Color online) Normalized collective ISFs for the large, $f_{bb}(q^*, t^*)$ (solid symbols), and small particles, $f_{ss}(q^*, t^*)$ (open symbols), calculated along *Path B* (as indicated) at fixed $q^* = 7.18$ as a function of the reduced time t^* . The upper panel displays the results from the SCGLE theory and the lower panel from MD simulations.

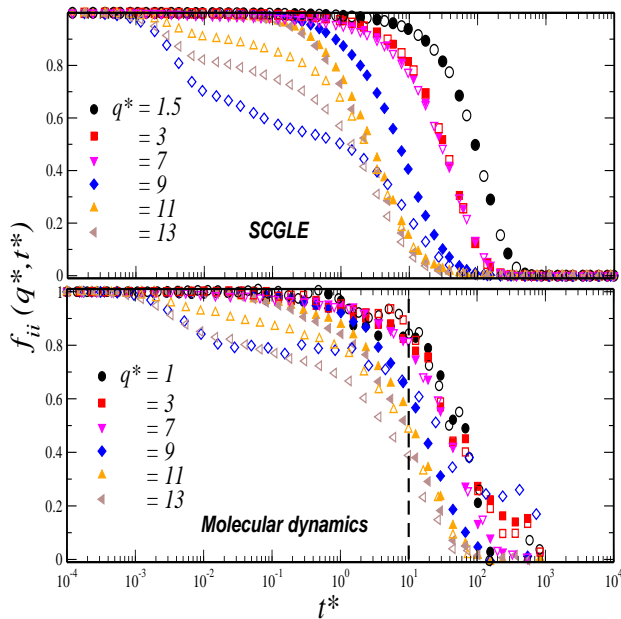


FIG. 14: (Color online) Normalized collective ISFs for the large, $f_{bb}(q^*, t^*)$ (solid symbols), and small particles, $f_{ss}(q^*, t^*)$ (open symbols), at the state point $b5 = (\phi_b = 0.45, \phi_s = 0.2)$, obtained from the SCGLE theory (upper panel) and MD (lower panel). The vertical dashed line in the lower panel indicates $t^* = 10$ at which the values $f_{ii}(q^*, t^* = 10)$ were extracted for the comparison in Fig. 3(b).

trated sample, $b5$ (Fig.14). For $q^* \leq 7$, both f_{bb} and f_{ss} decay rather similar, with a small *acceleration* of the dynamics of both species with increasing q^* . For $q^* > 7$, the relaxation time of both functions continues monotonically decreasing, which implies weak structural effects on the collective dynamics, as already suggested by the results in Fig. 3(b). Inflection points, followed by intermediate plateaus, are observed again in f_{ss} . The height of these plateaus, however, is significantly larger than those observed for the state point $a5$ (Fig.7).

To test the influence of ϕ_s on the q^* -dependence of the collective dynamics, we finally consider another route to the **F-DG** transition, in which ϕ_b is kept constant (at about 0.3) and ϕ_s is increased; *i.e.*, *Path 3*. The $f_{bb}(q^*, t^*)$ obtained from theory (Fig. 15) indicates a fluid behavior, with the relaxation becoming monotonously faster with increasing q^* , as observed at the state point $b5$. A similar situation is found for $f_{ss}(q^*, t^*)$, except for the distinct decay patterns observed for $q^* \geq 9.23$.

The SCGLE results are compared with experimental data (Fig. 16). Due to the limited measurement time (on the order of a day), the experimental data extend over a smaller time-window. Thus, the final decays of both $f_{bb}(q, t)$ and $f_{ss}(q, t)$ are not accessible in the experiments. Nevertheless, the trends are compatible with predictions by SCGLE. The initial relaxation of f_{bb} and f_{ss} is rather similar for $q^* \leq 7.06$, but with the later decaying faster for larger q^* , similar to the behavior found in both simulations (Fig. 14) and theory (Fig. 15). Approaching the **F-DG** transition line (*i.e.*, increasing ϕ_s), the decay of both f_{ss} and f_{bb} becomes noticeable slower at all length scales, in contrast with the behavior towards the **F-SG** transition (compare, for instance, the results of the lower panel of Fig. 16 against those of Figs. 9(b) and 9(c), all of which correspond to experimental *samples* where $\phi_b + \phi_s \approx 0.6$, but with significantly different compositions).

In summary, the results of this section show a different scenario towards the **F-DG** transition, where the *self* dynamics of the two species appear coupled and become slower simultaneously. The collective dynamics also appears coupled at all the relevant length scales, but display weak structural effects. These results indicate that both big and small spheres become arrested in the *self* and collective dynamics towards the **DG** domain.

VI. COMPARISON OF THE DYNAMICS TOWARDS THE **F-SG** AND **F-DG** TRANSITIONS

The self and collective dynamics approaching the **F-SG** and **F-DG** transitions have been described above and now will be compared. For this, notice that for each state point along *Path B*, there is a corresponding point along *Path A* having the same total volume fraction, ϕ , but a different composition $x_s \equiv \phi_s/\phi$. To highlight the corresponding samples, in Figs. 4-6 (*Path A*) and 11-13 (*Path B*) we have used the same symbols and colors for those state points with the same ϕ .

In Fig. 17, the evolution of the *self* dynamics along *Paths A* and *B* is compared in terms of the α -relaxation times $\tau_i^{\alpha,S}$, defined here as $F_{ii}^S(q^* = 7.18, \tau_i^{\alpha,S}) = 1/e$. For samples with the same ϕ , the relaxation of the small species is moderately

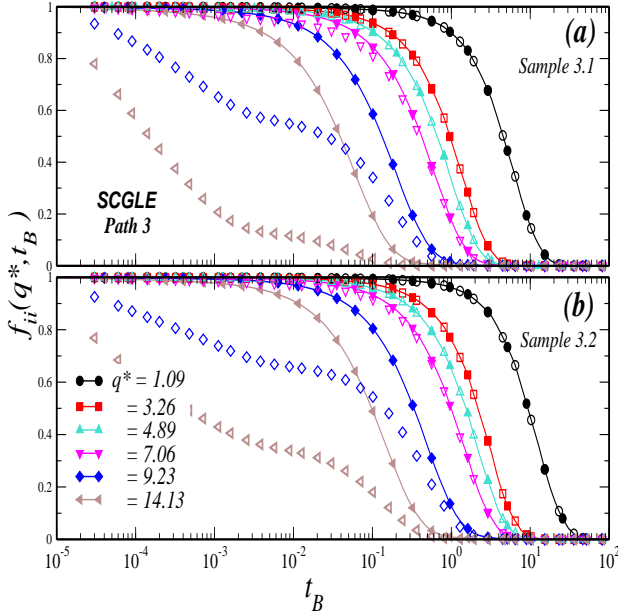


FIG. 15: (Color online) Normalized collective ISFs for (a) large, $f_{bb}(q^*, t_B)$, and (b) small particles, $f_{ss}(q^*, t_B)$, along *Path 3* for different reduced wave numbers q^* and fixed composition (*Sample 3.2*) as predicted by the SCGLE theory.

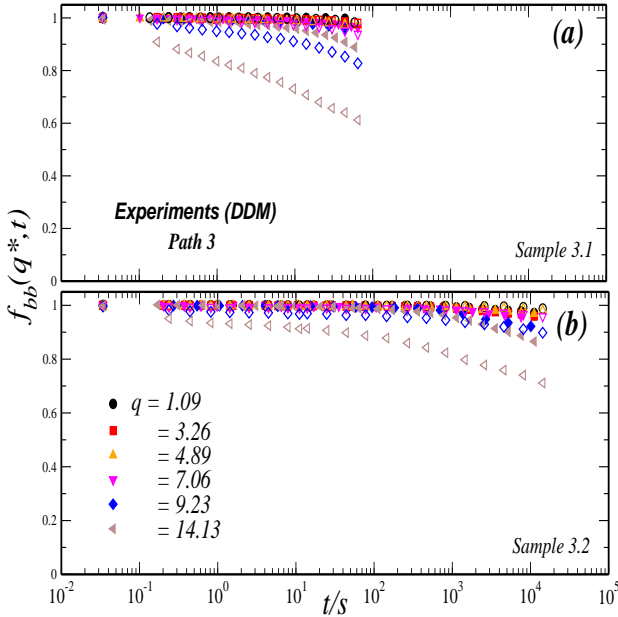


FIG. 16: (Color online) Normalized collective ISFs for (a) large, $f_{bb}(q^*, t)$, and (b) small particles, $f_{ss}(q^*, t)$, along *Path 3* for different reduced wave numbers q^* and fixed composition (*Sample 3.2*) as determined in experiments.

slower along *Path B* ($\phi_s = 0.2$) than *Path A* ($\phi_s = 0.05$), but displaying essentially the same dependence on ϕ . This indicates weak effects of the composition on the *self* dynamics of the small particles towards the glass transition, despite the different relaxation patterns observed in F_{ss}^S along *Paths A* (Fig.4) and *B* (Fig. 11). A distinct behavior for the large

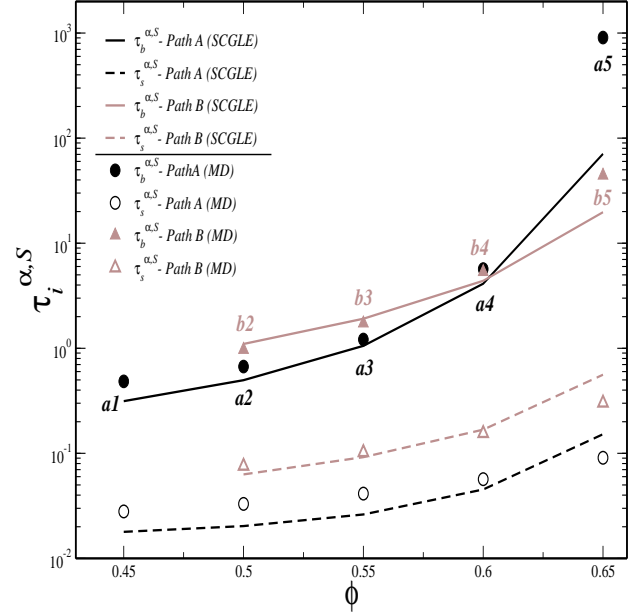


FIG. 17: (Color online) *Self* α -relaxation times of large (solid symbols, solid lines) and small particles (open symbols, dashed lines) along *Paths A* and *B* as a function of the total volume fraction ϕ . Symbols represent MD data and lines SCGLE results, as indicated.

species is found. For $\phi < 0.6$, the difference in the relaxation along both paths is smaller in comparison to the case of the small species, with the decay being again slightly slower along *Path B*. A crossover, however, is observed at $\phi \approx 0.6$ and, for larger $\phi (= 0.65)$, the relaxation becomes noticeable slower along *Path A*, which suggest strong effects of both composition and total concentration for the large particles' *self* dynamics.

To compare the collective dynamics close to the *F-SG* and *F-DG* transitions, we similarly consider collective relaxation times defined by $f_{ii}(q^*, t^* = \tau_i^\alpha) = 1/e$, for different q^* -values, and at the state points *a5* and *b5*, respectively (Fig. 18). For $q^* \leq 7.18$, the relaxation times of the small and large particles are strongly coupled for both compositions, with *Path B* displaying the slower relaxation for $q^* < 7$ and a crossover at $q \approx 7.18$ similar to the behavior of $\tau_i^{\alpha,S}$. At $q^* > 7.18$ and small x_s , *i.e.*, *many big particles* the relaxation of each species appears decoupled. The small species decay faster, indicating their ability to explore the local environment. If the fraction of the small particles is increased, the relaxation remains coupled, which reflects a more pronounced contribution of the small particles' dynamics to the slowing down.

VII. CONCLUDING REMARKS

By combining experiments, molecular dynamics simulations and theoretical calculations based on the SCGLE formalism, we have built up a general and consistent physical description of glassy dynamics in highly asymmetric binary mixtures of hard-spheres. Two fundamentally different sce-

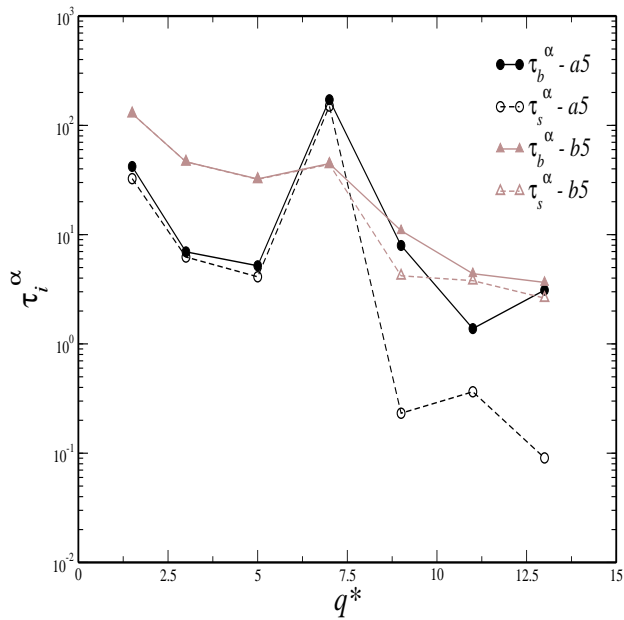


FIG. 18: (Color online) Collective α -relaxation times of both species as a function of reduced wave number q^* at the state points $a5$ (\bullet - τ_b^α , \circ - τ_s^α) and $b5$ (\blacktriangle - τ_b^α , \triangle - τ_s^α), as predicted by the SCGLE approximation.

narios for the glass transition were confirmed. Both lead to dynamical arrest; they are related to distinct microscopic states that, however, also bear similar qualitative features.

Below a certain volume fraction of small spheres, ϕ_s^E , a single glass occurs, where the slow dynamics is dominated by the large species and whose *self* and collective dynamics indicate structural arrest with the typical fingerprints of an ideal glass transition of hard spheres. In contrast, the *self* dynamics of the small species does not arrest, but resembles the behavior of a fluid embedded in a heterogeneous medium, including the long-time tail in the relaxation. Their collective dynamics at large length scales appeared coupled to the big particles and the dependence on the wave number follows the structure factor of the large particles, whereas at short length scales the dynamics remained ergodic. This is consistent with the following observation: the total volume fraction to reach the glass transition becomes larger with increasing the volume fraction

of small particles, ϕ_s .

In the other possible glass transition referred to as a double glass, the slowing down of the *self* and collective dynamics of both species appeared strongly correlated. In the latter case, the coupling occurred at all length scales, i.e., both species become dynamically arrested simultaneously. Contrary to the previous case, the total volume fraction at which the double glass transition occurs became smaller with increasing ϕ_s .

These fundamental differences when the mixture approaches to any glass boundary strongly suggest that the degrees of freedom of the small particles cannot be simply integrated out. For instance, assuming an effective potential between the large particles neglects the dynamical contribution of the small particles.

The above features were stressed out by all the techniques here employed, allowing to summarize our findings in a dynamical arrest diagram. Then, our results might serve to locate and reinterpret previous results in one of the possible glassy domains and as benchmark for future tests in colloidal hard sphere mixtures and other systems with competing time and length scales, such as metallic alloys, polymers or protein solutions. Finally, from a technological point of view, the understanding of arrested states will facilitate rational design of new materials, as well as many industrial processes.

Acknowledgments

This work was supported by the Consejo Nacional de Ciencia y Tecnología (CONACYT, Mexico) through grants Nos. 242364, 182132, 237425, 358254, FC-2015-2/1155, LANIMFE-279887-2017, and CB-2015-01-257636. L.F.E.A acknowledges financial support from the German Academic Exchange Service (DAAD) through the DLR-DAAD programme under grant No. 212. P. L. and S. U. E. acknowledge support by the German-Israeli Foundation (Grant No. J-1345-303.10/2016). R. C. P. acknowledges the financial support provided by Marcos Moshinsky Foundation, the University of Guanajuato (Convocatoria Institucional de Investigación Científica 2018), and the Alexander von Humboldt Foundation during his stay at the University of Düsseldorf in summer 2018.

-
- [1] A. L. Greer, *Science*, Vol. **267**, (1995) p. 1947-1953.
 [2] S. Zahid *et al.*, RSC Adv., 2016, **6**, 70197-70214
 [3] Y. Takahashi, Y. Yamazaki, R. Ihara and T. Fujiwara, *Sci. Rep.* **3**, 1147; DOI:10.1038/srep01147 (2013).
 [4] I. M. Hodge, *Science*, Vol. **267**, (1995) p. 1945-1947.
 [5] L. Cipelletti and L. Ramos, *J. Phys.: Condens. Matter* **17**, R253 (2005).
 [6] P.N. Segré, V. Prasad, A. B. Schofield, and D. A. Weitz, *Phys. Rev. Lett.*, **86**, No. 26, 6042 (2001).
 [7] P. J. Lu, E. Zaccarelli, F. Ciulla, A. B. Schofield, F. Sciortino and D. A. Weitz, *Nature*, 2008, 453 (7194) 499-503, doi: 10.1038/nature06931.
 [8] E. Zaccarelli and W.C. K. Poon (2009), *Proc. Natl. Acad. Sci. USA*, 106: 15203-15208.
 [9] A.P.R. Eberle, N.J. Wagner and R. Castañeda-Priego, *Phys. Rev. Lett.*, **106**, 105704 (2011).
 [10] C. A. Angell, *Science*, Vol. **267**, (1995) p. 1924-1935.
 [11] C. A. Angell, K. L. Ngai, G. B. McKenna, P. F. McMillan and S. F. Martin., *J. Appl. Phys.* **88**, 3113 (2000).
 [12] J. M. Lynch, G.C. Cianci and E. R. Weeks, *Phys. Rev. E*, **78**, 031410 (2008).
 [13] T. Narumi, S.V. Franklin, K.W. Desmond, M. Tokuyama and E.R. Weeks, *Soft Matter*, 2011, **7**, 1472-1482.
 [14] S. Vivek, C.P. Kelleher, P.M. Chaikin and E.R. Weeks, *Proc.*

- Natl. Acad. Sci. USA*, Vol. **114**, no.8, 1850-1855 (2017).
- [15] W. van Meegen and P.N. Pusey, *Phys. Rev. A*, **43**, No. 10, 5429, (1991).
- [16] W. van Meegen, S.M. Underwood and P.N. Pusey, *Phys. Rev. Lett.* **67**, No.12, 1587 (1991).
- [17] F. Sciortino and P. Tartaglia, *Adv. Phys.* **54**, 471 (2005).
- [18] G.L. Hunter and E.R. Weeks, *Rep. Prog. Phys.* **75** (2012) 066501.
- [19] A. Imhof and J. K. G Dhont, *Phys. Rev. Lett.*, **75**, No.8, 1662 (1997).
- [20] S.R. Williams and W. van Meegen, *Phys. Rev. E* **64**, 041502 (2001).
- [21] K.N. Pham, *et al.*, *Science*, Vol. **296**, 104 (2002).
- [22] K. N. Pham, S. U. Egelhaaf, P. N. Pusey, and W. C. K. Poon, *Phys. Rev. E* **69**, 011503 (2004).
- [23] T. Eckert and E. Bartsch, *Phys. Rev. Lett.* **89**, 125701 (2002).
- [24] T. Sentjabrskaja, M. Hermes, W. C. K. Poon, C. D. Estrada, R. Castañeda-Priego, S.U. Egelhaaf and M. Laurati, *Soft Matter*, 2014, **10**, 6546.
- [25] J. Hendricks, R. Capellmann, A. B. Schofield, S. U. Egelhaaf, and M. Laurati, *Phys. Rev. E* **91**, 032308 (2015).
- [26] A. Meyer *Phys. Rev. B*, **66** 13425, (2002).
- [27] Th. Voigtmann, A. Meyer, D. Holland-Moritz, S. Stüber, T. Hansen and T. Unruh, 2008 *EuroPhys. Lett.* **82** 66001
- [28] E. R. Weeks and D. A. Weitz, *Phys. Rev. Lett.*, Vol. **89** 095704 (2002).
- [29] T. Sentjabrskaja, *et al.*, *Nat. Comm.* **7**:11133 doi: 10.1038/ncomms11133 (2016).
- [30] D. Heckendorf, K.J. Mutch, S.U. Egelhaaf and M. Laurati, *Phys. Rev. Lett.*, **119**, 048003 (2017).
- [31] A.J. Moreno and J. Colmenero, *J. of Chem Phys* **125**, 164507 (2006).
- [32] C. Mayer, F. Sciortino, C.N. Likos, P. Tartaglia, Hartmut Löwen and E. Zaccarelli, *Macromolecules*, 2009, **42**(1), pp 423-434.
- [33] Th. Voigtmann and J. Horbach, *Phys. Rev. Lett.* **103**, 205901 (2009).
- [34] L. Fabbian, W. Götze, F. Sciortino, P. Tartaglia, and F. Thiery, *Phys. Rev. E*, **59**, No.2 R1347 (1999).
- [35] J. Bergenholtz and M. Fuchs, *Phys. Rev. E*, **59**, No.5, 5709, (2009).
- [36] K.A. Dawson, *Curr. Opin. Colloid Interf. Sci.* **7**, 218 (2002).
- [37] N. Khali, A. de Candia, A. Fierro, M. Pica Ciamarra and A. Coniglio, *Soft Matter*, 2014, **10**, 4800.
- [38] E. López-Sánchez, C. D. Estrada-Alvarez, G. Pérez-Angel, J. M. Méndez-Alcaraz, P. González-Mozuelos and R. Castañeda-Priego, *J. Chem. Phys.* **139**, 104908 (2013).
- [39] C. Grodon, M. Dijkstra, R. Evans, R. Roth, *J. Chem. Phys.*, **121**, 7869 (2004).
- [40] W. Götze, in *Liquids, Freezing and Glass Transition*, edited by J. P. Hansen, D. Levesque, and J. Zinn-Justin (North-Holland, Amsterdam, 1991).
- [41] W. Götze and L. Sjögren, *Rep. Prog. Phys.* **55**, 241 (1992).
- [42] W. Götze, *Condensed Matt. Phys.*, 1998, Vol. 1, No. 4(16), p. 873-904.
- [43] W. Götze, *Complex Dynamics of Glass-Forming liquids. A Mode-coupling theory*, Oxford University Press (2009).
- [44] L. Yeomans-Reyna and M. Medina-Noyola, *Phys. Rev. E*, **640**, 066114 (2001).
- [45] L. Yeomans-Reyna, *et al.*, *Phys. Rev. E* **76**, 041504 (2007).
- [46] M. A. Chávez-Rojo and M. Medina-Noyola, *Phys. Rev. E* **72**, 031107 (2005), *Phys. Rev. E* **76**, 039902 (2007).
- [47] R. Juárez-Maldonado *et al.*, *Phys. Rev. E* **76**, 062502 (2007).
- [48] R. Juárez-Maldonado and M. Medina-Noyola, *Phys. Rev. E.*, **77**, 051503 (2008).
- [49] R. Juárez-Maldonado and M. Medina-Noyola, *Phys. Rev. Lett.* **101**, 267801 (2008).
- [50] Th. Voigtmann and W. Götze, *Phys. Rev. E*, **67**, 021502 (2003).
- [51] Th. Voigtmann, 2011 *EuroPhys. Lett.* **96**, 36006.
- [52] J. K. Percus and G. J. Yevick, *Phys. Rev.*, **110**, 1 (1957).
- [53] L. Verlet and J.-J. Weis, *Phys. Rev. A*, **5**, 939 (1972).
- [54] L.F. Elizondo-Aguilera and M. Medina-Noyola, *J. Chem. Phys.*, **142** 224901 (2015).
- [55] E. Lázaro-Lázaro, P. Mendoza-Méndez, L.F. Elizondo-Aguilera, J.A. Perera-Burgos, P. E. Ramírez-González, G. Pérez-Ángel, R. Castañeda-Priego and M. Medina-Noyola, *J. Chem. Phys.*, **146** 184506 (2017).
- [56] M. C. Vargas and G. Pérez-Ángel, *Phys. Rev. E*, **87**, 042313 (2013).
- [57] P. E. Ramírez-González and M. Medina-Noyola, *Phys. Rev. E* **82**, 061503 (2010).
- [58] L. E. Sánchez-Díaz, E. Lázaro-Lázaro, J. M. Olais-Govea and M. Medina-Noyola, *J. Chem Phys.* **140**, 234501 (2014).
- [59] P. Mendoza-Méndez, E. Lázaro-Lázaro, L. E. Sánchez-Díaz, P. E. Ramírez-González, G. Pérez-Ángel, and M. Medina-Noyola, *Phys. Rev. E* **96**, 022608 (2017).